Agglomeration of stoichiometric hydroxyapatite: Impact on particle size distribution and purity in the precipitation and maturation steps

M. Tourbin [a], F. Brouillet [b], B. Galey [a], N. Rouquet [c], P. Gras [a], N. Abi Chebel [b], D. Grossin [b], C. Frances [a, *]

[a] Laboratoire de Génie Chimique (LGC), Université de Toulouse, CNRS, 4 Allée Émile Monso, 31432, Toulouse Cedex 4, France
[b] CIRIMAT, Université de Toulouse, CNRS, 4 Allée Émile Monso, 31432, Toulouse Cedex 4, France
[c] URODELIA Company, 416 route de saint-Thomas, 31470, Saint-Lys, France

ARTICLE INFO

ABSTRACT

Stoichiometric hydroxyapatite (HAP) is a prominent biomaterial, notably used as coating on metal bone prostheses. High chemical purity and a specific particle size distribution are the main properties for such an application. Based on industrial practice, a reference synthesis was first performed in a lab scale stirred reactor. Improvements were then suggested by varying the physicochemical and hydrodynamic conditions. The shear rate within the reactor, characterized by the mean Kolmogorov micro scale, has a strong impact on the final agglomerate size distribution. By maintaining a rather high mixing rate and a high temperature, the duration of the synthesis can be reduced considerably without affecting the HAP purity provided the pH is properly regulated. This consists of imposing acidic conditions during a short period just after the initial formation of large aggregates and then setting the pH at above 7.5 to ensure the production of pure stoichiometric HAP.

1. Introduction

Calcium phosphate ceramics constitute an important class of privileged materials because of their strong similarities with the mineral component of natural bone [1]. Hydroxyapatite (HAP) is one of these prominent biomaterials, used as coatings on metal bone prostheses [2]. It has the ability to improve the quality of the bone/implant interface and to promote osseointegration. HAP is usually synthesized as a powder and applied to the metal surface by means of plasma spraying. In order to obtain high quality coatings, it is necessary to control the properties and characteristics of the hydroxyapatite powder used in the plasma spray coating method. The chemical composition and density of the hydroxyapatite powder, as well as the particle size and morphology, are properties that affect the quality of the final coating [3]. Several methods have been developed for HAP synthesis, including mechanochemical or solid state reaction, precipitation, hydrothermal and sol gel routes, and various deposition techniques [4,5]. Precipitation is the most cost effective of these techniques, and hence is the most widely used at industrial scale. Industrial processes based on hydroxyapatite precipitation often include the successive steps of precipitation, maturation, washing, spray drying and calcination/sintering. Maturation of the HAP suspension is usually carried out in order to improve the HAP crystallinity and/or the size and shape of the crystals [6,7] while the spray drying operation allows large dried agglomerates or granules to be produced, the morphology of which can be controlled by acting on the process parameters [8]. Finally, the physical characteristics of the powder result from the agglomeration phenomena that take place during the different processing steps of the particles initially produced by precipitation following a growth mechanism by nucleation aggregation agglomeration as described by Rodriguez Clemente et al. [9].

Industries face low yields due to loss of the finest particles at certain steps of the process (washing, spraydrying, etc.). Similarly, oversized particles are removed during the final sieving, which leads to a consequent loss of material. In order to solve this performance problem, one solution is to promote the agglomeration of the majority of the finer particles, thus preventing their evacuation during the washing operation. The production of a monodisperse powder, which results from controlled agglomeration, also allows the amount of oversized material to be reduced. The powder properties depend on the operational conditions during the HAP synthesis and the successive operations. We will focus on the precipitation and maturation phases here. The effect of the physicochemical parameters on the HAP crystallinity and crystallite size has been intensively studied in the literature. It is known that higher crystallinity is obtained by increasing the temperature. In fact, the HAP formation reaction comprises several successive steps: first the formation of octacalcium phosphate (OCP), which is rapidly transformed into amorphous calcium phosphate (ACP), which is then converted into HAP [10]. Low crystallinity may thus be observed during the first period of the precipitation with the existence of precursors such as OCP and ACP [9]. Temperature strongly affects the conversion rate of ACP to HAP [10,11]. For example, Liu et al. [10] reported that 1 day was needed to form pure HAP by adding 1 mol/l of $Ca(NO_3)_2$

• Corresponding author.
E-mail address: christine.frances@ensiacet.fr (C. Frances).

https://doi.org/10.1016/j.powtec.2019.10.050
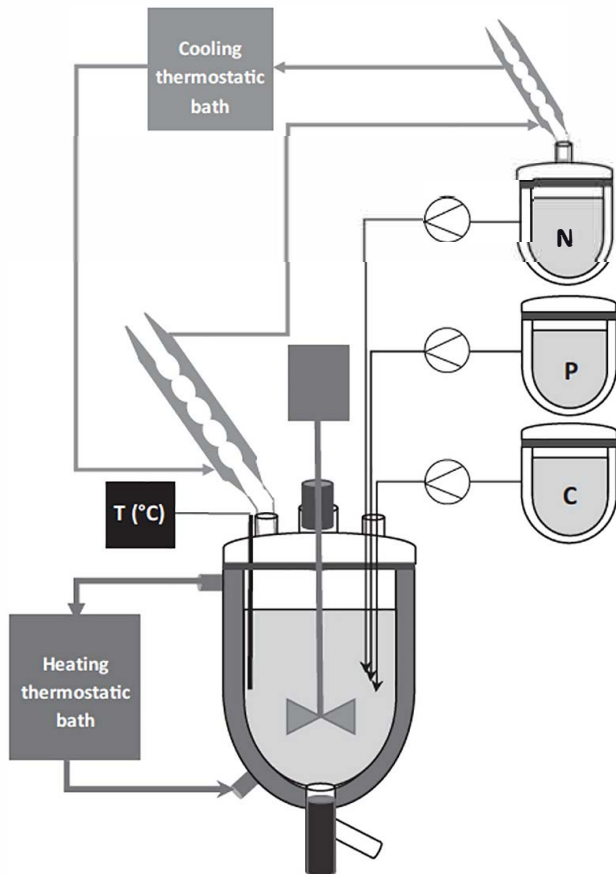
Fig. 1. Lab-scale reactor for HAP process synthesis.

[6,10,11]. The crystallite size thus increases with the temperature but, since high temperatures promote nucleation, the particles also tend to agglomerate with each other and larger mean sizes of agglomerate are observed [11]. The reaction pH has also an important effect on the properties of HAP. Most studies dealing with pure HAP synthesis have been conducted at a basic pH, kept constant during the process or adjusted at the beginning of the synthesis by adding ammonia or ammonium hydroxide [6 10,12,13]. Analysing the effect of pH during the synthesis of HAP by adding orthophosphoric acid drop by drop into a calcium hydroxide solution, Afshar et al. [14] recommend adjusting the pH level to at least 7.5 to obtain pure HAP. Al Qasas and Rohani [11] show that, in the range (7 11), the pH acts more on the size and morphology of the particles than on the HAP crystallinity. The concentration of the reactants and their feeding rates also have an impact on the reaction kinetics and, together with the temperature and pH conditions, have an effect on the crystal size and shape. The hydrodynamic conditions may also influence HAP properties, in particular the agglomerate particle size distribution, but they have been much less analysed than the physicochemical conditions.

Here we focus on the study of particle agglomeration during the precipitation and maturation steps in order to control the size of the aggregates. The aim of this work is to analyse the impact of different synthesis conditions on stoichiometric hydroxyapatite (HAP) agglomeration in order to improve the process in terms of product quality (purity, aggregate size distribution and morphology) and process yield.

2. Material and methods

The precipitation of hydroxyapatite was performed in a stirred tank and resulted from the reaction of phosphoric acid 85% (Carlo Erba Reagents) and calcium nitrate 4-hydrate crystals, ~17% Ca (Dr. Paul Lohmann manufacture) at a high temperature in an aqueous ammonia medium, 28% (Carlo Erba Reagents). The global equation may be written as:

$$10Ca(NO_3)_2, 4H_2O + 6(NH_4)_2HPO_4 + 8(NH_4)OH$$
$$\rightarrow Ca_{10}(PO_4)_6(OH)_2 + 20NH_4NO_3 + 6H_2O \tag{1}$$

2.1. Experimental set-up

The lab-scale apparatus used for the synthesis is illustrated in Fig. 1. It was composed by a double-jacketed cylindrical glass vessel, 1 L in capacity, and three glass containers for
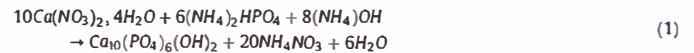
and 1 mol/l of (NH)₂HPO at 25 °C and at pH (10 11), whereas, at 95 °C, only 5 min were required. At a low temperature, a maturation step is often necessary to obtain thermally stable HAP [6]. The temperature also has a marked impact on the size and the morphology of the precipitated HAP
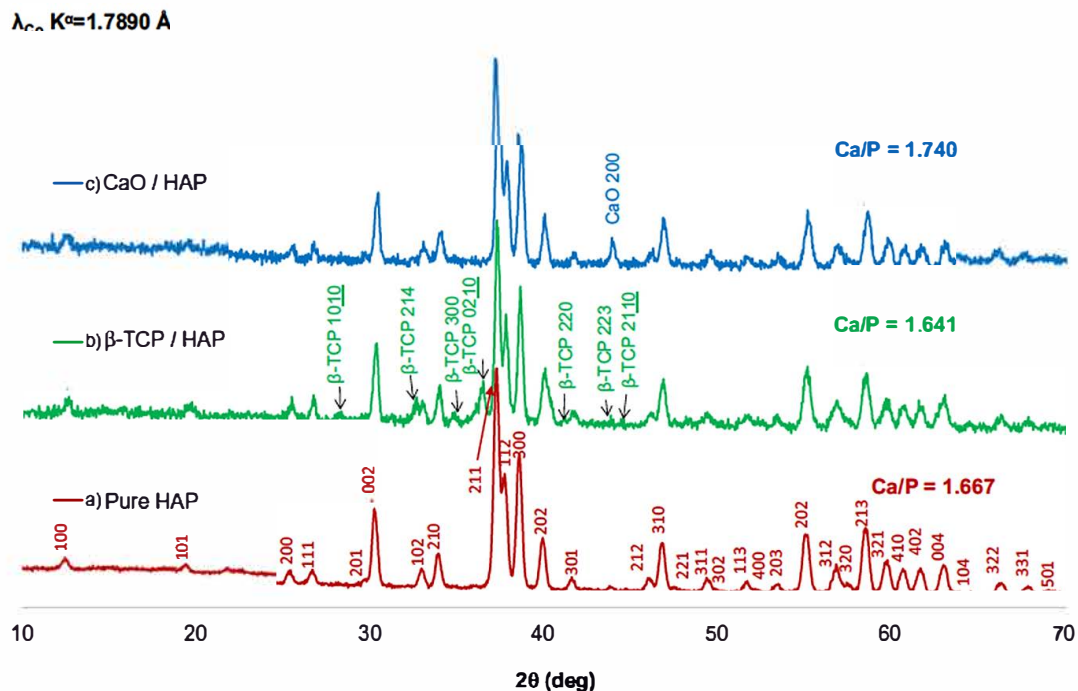

Fig. 2. Characteristic X-ray diffractograms and corresponding Ca/P ratios for pure HAP (a) or mixed products β–TCP/HAP (b) and CaO/HAP (c).
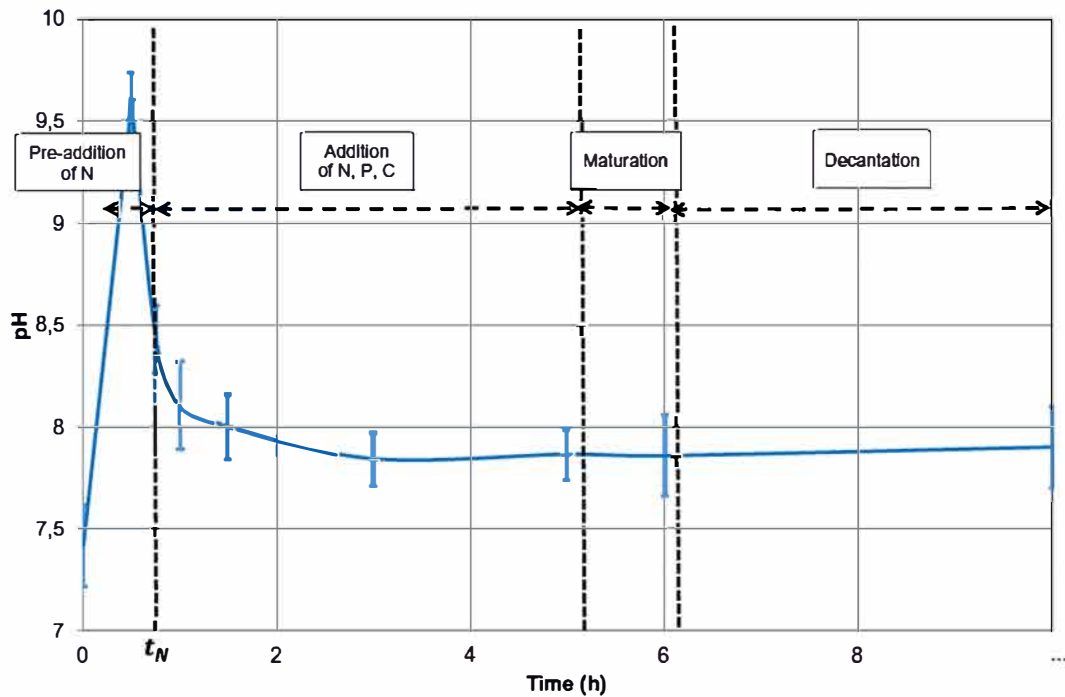
Fig. 3. Change of pH over time for a standard synthesis (Run 1).

the reactants. The reactor had three baffles and was equipped with a three-blade Lightning A310 axial stirrer, which had a diameter of 6 cm and was located a third of the way up of the reactor.

Initially, a given volume of calcium nitrate aqueous solution (14 wt%) was poured into the reactor, then brought to the desired synthesis temperature. Three solutions, labelled C, P and N, held in the three vessels, were then continuously introduced into the reactor by means of peristaltic pumps operating at fixed flow rates. Solution C was an aqueous solution at 32.1 wt% of calcium nitrate. Solution P was a mixture of phosphoric acid at 85% (15.3 wt%), ammonia at 20.5% (5.73 wt%) and water. Solution N contained only ammonia at 20.5%. The three reactants were maintained at room temperature and a cooler was used to condense the ammonia vapour present in the top of the reactor. During the first period of the synthesis process, only solution N was supplied in order to increase the pH of the solution inside the reactor. Then, during the second period, in which the synthesis itself was performed, the three solutions were fed in continuously. At the end of the synthesis, the supply of reactants and ammonia solution was stopped but the reaction medium was maintained under stirring at high temperature during the maturation phase. The reactor was drained and the suspension was poured into a vessel where it was kept at room temperature for several hours to allow suspended agglomerates to settle. After decantation, the particles were washed during the filtering of the suspension, which was done by suction through a Buchner funnel using a filter paper. The filtration cake was freezedried then calcined in an oven at 1000 °C for 10 h for characterization purposes. This final step dried the crystallized HAP and removed any remaining impurities. The temperature and time conditions imposed during calcination also guaranteed the decomposition of the product and allowed the different phases to be quantified by X-ray diffraction. For analysis
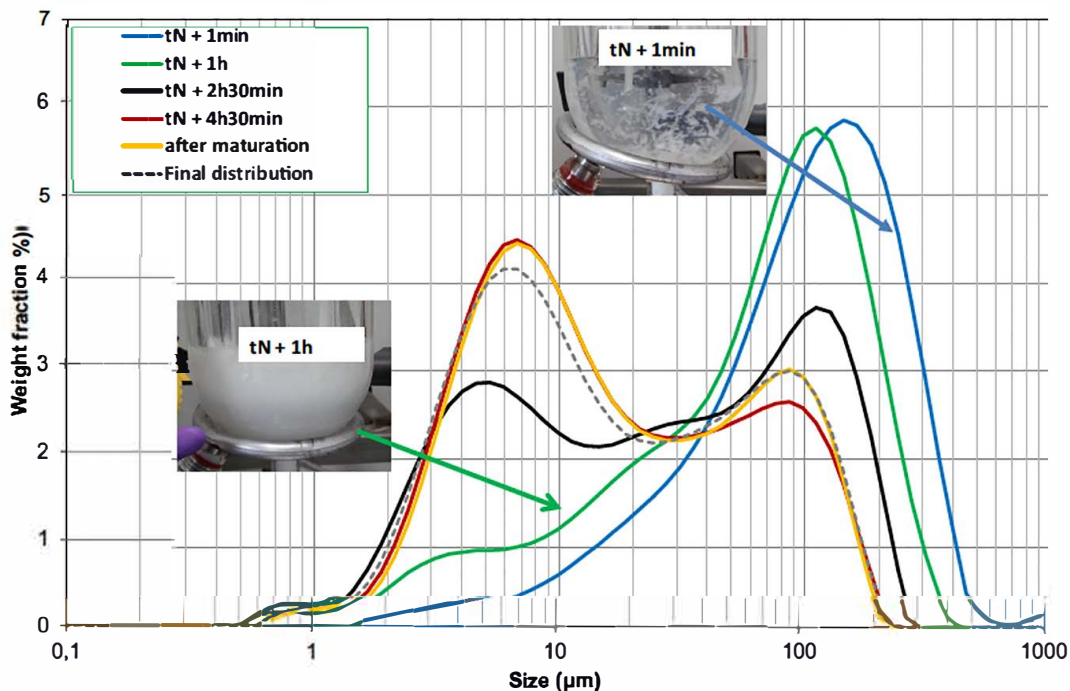

Fig. 4. Change of the particle size distribution over time during a standard synthesis (Run 1).
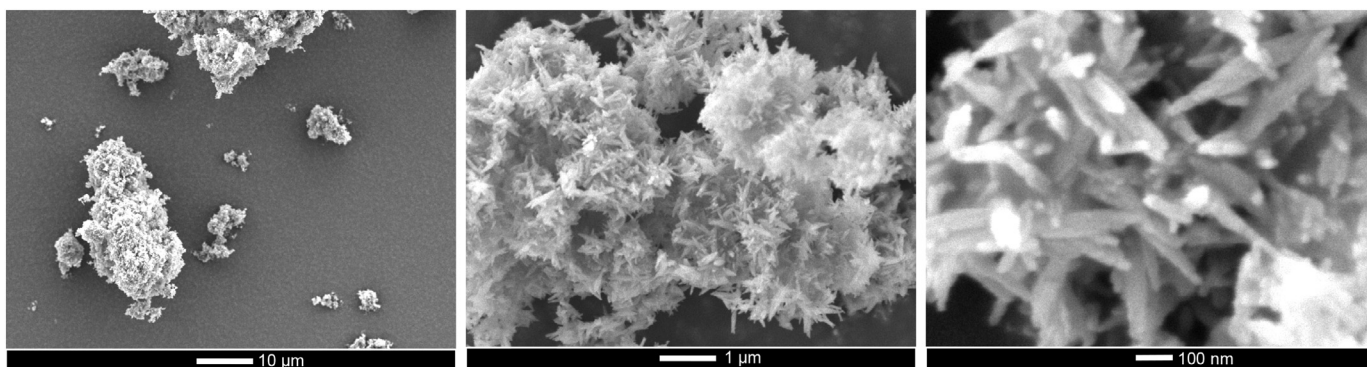
Fig. 5. SEM photos of the agglomerated powder recovered after a standard synthesis.

purposes, samples of the slurry were also collected throughout the process. They were used for particle size distribution measurement and pH analysis or to provide dried or calcined powders for evaluation of the HAP purity.

2.2. HAP properties

The size distribution of the suspended particles was determined by laser diffraction using a Mastersizer 3000 (Malvern Instruments Ltd.). The pH of the suspension was also measured on slurry samples taken during the synthesis. Since the pH is sensitive to the temperature, the correlation between them was determined previously. A linear, decreasing function was observed. The temperature at which the pH was measured could also vary depending on the time that elapsed between the sampling and the measurement so, and in order to avoid any bias and allow an accurate comparison of the results,

whatever this temperature was, the values reported in this paper were obtained by conversion to the temperature imposed during the synthesis process.

The purity of the product (standard ISO 13779-3: 2008) was checked by X-ray diffraction (Equinox 1000, INEL) after its calcination at 1000 °C for one night (10–15 h). In such conditions, only the products with a stoichiometric ratio Ca/P = 1.67 are stable: the other compounds decompose into HAP and CaO (if the ratio Ca/P > 1.667) or HAP and β-TCP (for a ratio Ca/P < 1.667) during calcination. Some typical indexed diffractograms are reported in Fig. 2 for pure HAP powder (Fig. 2a) and for mixed materials containing β-TCP and HAP (Fig. 2b) or CaO and HAP (Fig. 2c). HAP, α-TCP, β-TCP and CaO are identifiable according to the lines given the sheets JCPDS 09–0432, JCPDS 09–0348, JCPDS 09–0169 and JCPDS 04–0777 (standard ISO 13779-3: 2008) respectively. After quantification of the HAP, TCP or CaO content in the calcined sample, the molar ratio between calcium and phosphorous in the sample (Ca/P) was calculated using the following equation, based on the chemical formula of HAP, TCP and CaO.

Table 1
Hydrodynamic characteristics for the reactor.

N (rpm)	120	300	600
Re	7200	18000	36000
G (s^{-1})	43	171	483
$\langle\varepsilon\rangle$ (m^2.s^{-3})	1.8×10^{-3}	2.9×10^{-2}	2.3×10^{-1}
$\langle\eta\rangle$ (μm)	152	77	45

$$Ca/P = \frac{n_{Ca}}{n_P} = \frac{\dfrac{10}{M_{HAP}}w_{HAP} + \dfrac{3}{M_{TCP}}(w_{\alpha-TCP} + w_{\beta-TCP}) + \dfrac{1}{M_{CaO}}w_{CaO}}{\dfrac{6}{M_{HAP}}w_{HAP} + \dfrac{2}{M_{TCP}}(w_{\alpha-TCP} + w_{\beta-TCP})}$$

$$(2)$$

where n_x is the mole number of product x, M_x its molar weight, and w_x its mass fraction.

To meet the standard, the HAP powder was expected to be at least 95% pure and thus contain less than 5% of β-TCP or CaO. Since the Ca/P ratio of stoichiometric hydroxyapatite is equal to 1.667, it was considered acceptable for this ratio to lie between 1.658 (which corresponds to a HAP powder containing 5% of β-TCP) and 1.824 (HAP powder + 5% CaO).
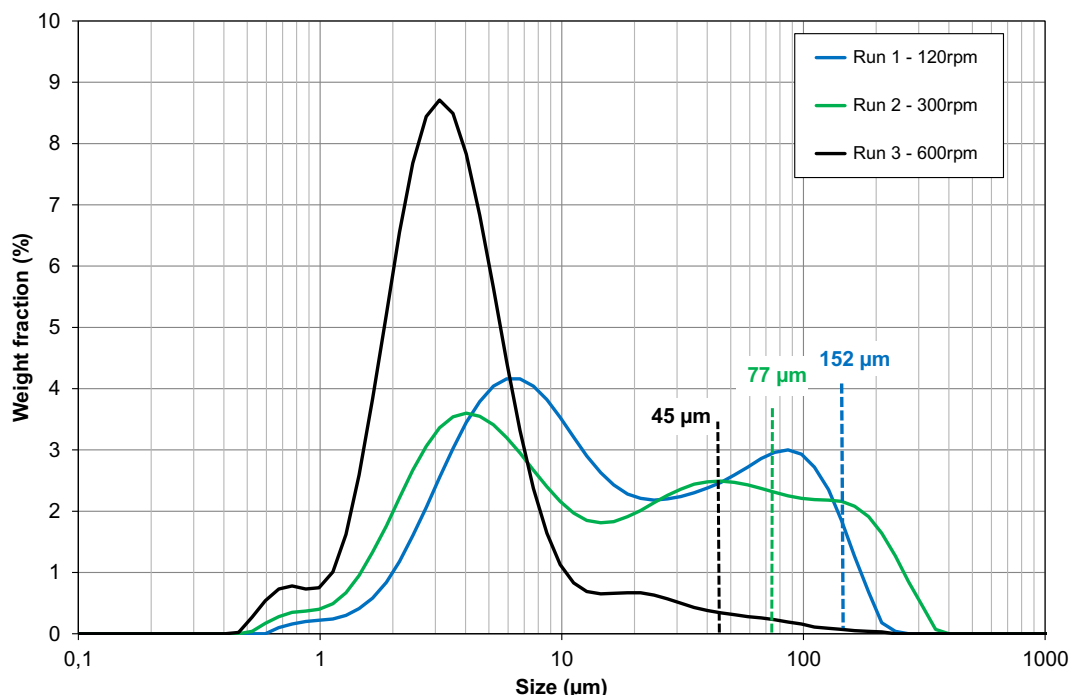

Fig. 6. Effect of the hydrodynamic conditions on the size distribution of the product recovered at the end of the synthesis process.

Table 2
Run conditions and Ca/P ratios derived from X-ray analysis on calcined powder.

Run label	Stirring rate	Global synthesis duration	Pre-addition of N duration	Addition of N, P, C duration	N flow conditions	Maturation duration and conditions	pH control	Ca/P
Run 1	120 rpm	t - 5 h	30min	4 h30min	N	1 h–120 rpm	NO	1.641
Run 2	300 rpm	t - 5 h	30min	4 h30min	N	1 h–300 rpm	NO	1.682
Run 3	600 rpm	t - 5 h	30min	4 h30min	N	1 h–600 rpm	NO	1.670
Run 4	600 rpm	t/2 - 2 h30	15min	2 h15min	N	30min–600 rpm	NO	1.667
Run 5	600 rpm	t/4 - 1 h15	7.5min	1 h7min30s	N	15min–600 rpm	NO	1.667
Run 6	600 rpm	t/10 - 30min	instantaneous	30min	N	NO maturation	NO	1.667
Run 7	600 rpm	t/20 - 15min	instantaneous	15min	N	NO maturation	NO	1.667
Run 8	600 rpm	t/inst - 1min	instantaneous	1min	N	NO maturation	NO	1.667
Run 9	300 rpm	t/10–30min	instantaneous	30min	N	1 h30 – 300 rpm	NO	–
Run 10	300 rpm	t/10–30min	instantaneous	30min	N	1 h30 – 600 rpm	NO	–
Run 11	300 rpm	t/2 - 2 h30	15min	2 h15min	N	30min–300 rpm	NO	1.667
Run 12	300 rpm	t/2 - 2 h30	15min	2 h15min	Nx1.4	30min–300 rpm	NO	1.667
Run 13	300 rpm	t/2 - 2 h30	15min	2 h15min	Nx3	30min–300 rpm	NO	1.685
Run 14	600 rpm	t/10 - 30min	instantaneous	30min	N	NO maturation	pH = 8	1.664
Run 15	600 rpm	t/10 - 30min	instantaneous	30min	N	NO maturation	pH = 9	1.687
Run 16	600 rpm	t/10 - 30min	instantaneous	30min	N	NO maturation	pH Reg	1.660

3. Results and discussion

3.1. Reference synthesis results

Standard conditions, similar to those used in industrial practice, were chosen to define a reference synthesis (Run 1). The total duration of the synthesis process (corresponding to the first and the second periods) was fixed at 5 h. It was conducted at 75 °C under a moderate agitation speed (120 rpm). This temperature was chosen for kinetic and thermodynamic purposes in order to obtain thermally stable HAP [3,6]. During the first 30 min, the feed comprised only the ammonia solution N. Then the three solutions P, C and N were fed for the remaining time, keeping their flow rates constant. They were chosen in the ranges of (45–50 ml/h) for Solution P, (35–40 ml/h) for Solution C and (25–30 ml/h) for Solution N. After the end of the supply of reagents, the suspension was kept at the same temperature and stirred for one extra hour (maturation step). The next steps (decantation, washing, filtration, drying and calcination) were performed as described previously.

Without any pH regulation, a characteristic change was observed in the pH of the suspension over time, as illustrated in Fig. 3. In the first 30 min, during which only the ammonia solution was fed, the pH increased considerably. Immediately after the other two reactants began to be supplied, the pH decreased for approximately 1 h, quickly during the first few minutes then more slowly, and finally tended to stabilize until the end of the synthesis process.

The change of the particle size distribution over the synthesis time is shown in Fig. 4. The particle size distributions are multimodal and spread over three decades, from approximately 1 μm to about 1 or more millimetres. Surprisingly, they moved from the right (larger sizes domain) to the left part (smaller sizes domain) during the process. The first sample (labelled t_N +1min) was taken 1 min after the beginning of the supply of the two reagents (phosphoric acid and calcium nitrate). A white precipitate, composed of large flocs, was observed in the reactor with the naked eye (cf. photo of the reactor labelled "t_N + 1min" inserted in Fig. 4). As mentioned in the introduction, it is known that the HAP formation reaction comprises several steps [10]. An intermediate amorphous phase may appear before its conversion into HAP. Afterwards, smaller agglomerates were obtained and the solution turned milky (cf. photo labelled "t_N + 1 h" inserted in Fig. 4) as physicochemical and hydrodynamic conditions favoured the agglomeration of crystallites and agglomerates of different sizes appeared. However, the shear induced by the agitator could also cause the agglomerates to break. The relationship between hydrodynamic conditions and aggregate size will be analysed in more detail later. During the maturation step, the particle distribution seemed to evolve but to a lesser extent. This point will also be discussed later.

Some relevant SEM photos of the dried powder recovered at the end of the synthesis are reported in Fig. 5. The dried powder seems to be composed of coarse agglomerates of ten microns or more, composed of a disordered assembly of acicular crystallites a few hundred nanometres in length and about 50 nm in width.

The product composition was determined on calcined samples taken throughout the synthesis process. It was thus possible to evaluate the Ca/P ratio as a function of the progress of the synthesis reaction, by comparing the X-ray diffractograms with that of pure HAP. Ca/P ratios of 1.740, 1.721, 1.658 and 1.641 were obtained on calcined powder for samples recovered after 1.5, 3 and 5 h, and at the end of the synthesis, respectively. Thus, the powder composition changed as the reaction progressed. CaO was detectable in the sample taken after 1.5 h of the synthesis process. Its proportion then decreased until 3 h had elapsed, and it finally disappeared. Meanwhile, characteristic peaks relative to β-TCP appeared. The presence of CaO at the initiation of the process can be easily explained by the fact that the reactor contents were initially calcium nitrate and water. Calcium was thus present in excess compared to phosphorous and, consequently, a high Ca/P ratio was observed. The progress of the process then rectified this excess and the ratio decreased. The appearance of the under-stoichiometry at the end of the synthesis is more

problematic. It was probably due to poor mixing of the reactor contents as the useful volume inside the container increased over the synthesis process. The impact of the stirring conditions on the HAP properties was analysed and is discussed in the next section.

In addition, samples of about 20 ml were collected during the synthesis and then washed, filtered and freeze dried. The quantity of powder was weighed and compared to the theoretical amount expected according to the progress of the synthesis process. It is interesting to note than the yield was constant during the whole synthesis process. Finally, a total of about 54 g of powder (with a moisture content of 10%) was recovered, which corresponds to a yield higher than 98%. The reaction was thus complete and quasi instantaneous.

3.2. Effect of the stirring rate applied during the synthesis

Under the given process conditions, it was observed that the initial agglomerates (cf. Fig. 4 at t_N +1) had a rather large and dispersed size. The size then decreased during the synthesis, probably thanks to breakage and restructuring. Another conclusion of this reference trial is that the mixing of the reaction media has to be efficient enough to homogenize the reactants throughout the synthesis process. Therefore the impact of the hydrodynamic conditions on the HAP properties was analysed in a series of 3 trials. The stirring rate was set in the range of (120–600 rpm), higher than the stirring rate chosen for the reference synthesis, which was set at 120 rpm. The stirring speed was kept fixed at the chosen value during the syntheses (Runs 1, 2 or 3), as were other geometric conditions (impeller type and size, impeller height from the reactor bottom, number of baffles). In an agitated reactor, the hydrodynamics is often characterized by the Reynolds Number (Re) and the global velocity gradient (G) [s^{-1}] defined as:

$$Re = \frac{N d_a^2}{\nu} \tag{2a}$$

$$G = \sqrt{\frac{P}{\rho \nu V}} \tag{3}$$

where N is the impeller frequency [rpm], d_a the impeller diameter [m], ν the kinematic viscosity [m^2. s^{-1}], P [W] the global power dissipated in the reactor, V the volume of the suspension [m^3] and ρ its density [kg.m^{-3}]. The power dissipated can be deduced from the power number (N_p) of the impeller (depending on the flow regime and the impeller type; a value of 0.3 was assumed in this study) given by:

$$N_p = \frac{P}{\rho N^3 d_a^5} \tag{4}$$

The power dissipated is related to the global viscous dissipation rate of the turbulent kinetic energy $\langle \varepsilon \rangle$ [m^2. s^{-3}] by:

$$\langle \varepsilon \rangle = \frac{P}{\rho V} \tag{5}$$

So the global velocity gradient can also be written as:

$$G = \sqrt{\frac{\langle \varepsilon \rangle}{\nu}} \tag{6}$$

Several authors [15] have pointed out that, during a flocculation process, the floc size is close to the Kolmogorov microscale (η), which is the size of the smallest eddies present in the flow. In the present study, the mean Kolmogorov microscales $\langle \eta \rangle$ were estimated on
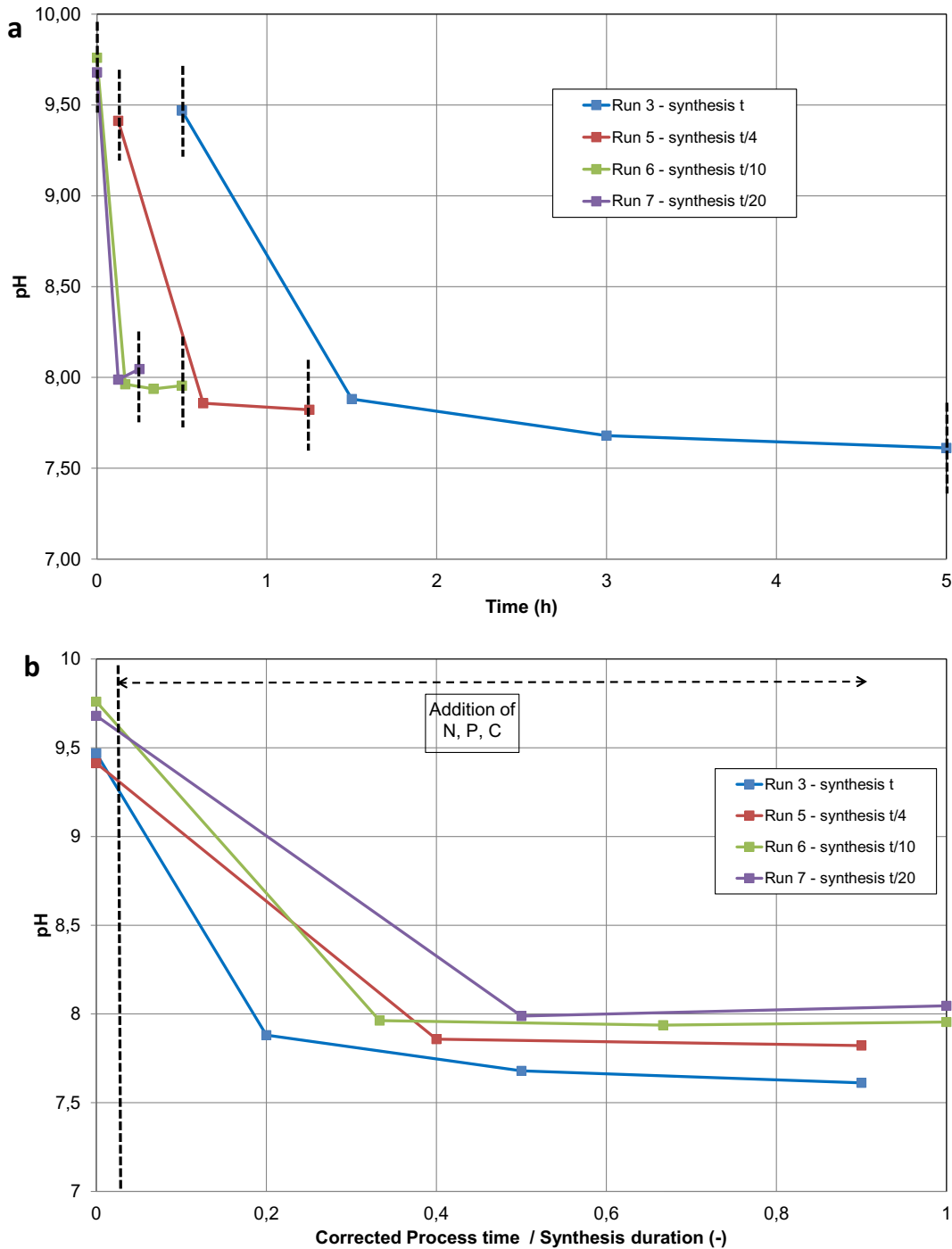
Fig. 7. Change of pH over time depending on the reactant flow rates. a) Change of pH over time from the beginning of reactant feeds until the end. b) Change of pH over the dimensionless process time depending on synthesis duration.

the basis of the global viscous dissipation rates $\langle\varepsilon\rangle$ and for the different impeller velocities through the following equation:

$$\langle\eta\rangle = \left(\frac{\nu^3}{\langle\varepsilon\rangle}\right)^{1/4} \quad (7)$$

The values of Re, G, $\langle\varepsilon\rangle$ and $\langle\eta\rangle$ are reported in Table 1. The volume of the suspension was considered to be 1×10^{-3} m^3 and the kinematic viscosity was taken as 1×10^{-6} m^2 s^{-1}. The suspension density was 1125 kg m^{-3} at the end of the synthesis.

It can be concluded that the flow regime was turbulent for the values of the stirring rate considered.

Whatever the stirring rate applied during the synthesis, the changes of the particle size distribution versus time were similar to those observed during the standard synthesis,

characterized by a decrease of the particle size versus time, but the kinetics increased with the stirring speed. The size distributions of the product at the end of the synthesis step are shown in Fig. 6. Whatever the stirring rate applied during the synthesis, the size distribution of the product recovered at the end of the synthesis process was multimodal. The majority of particles were a few microns in size, with a greater or lesser proportion of larger agglomerates. A sub population of submicronic particles was also observed. The particle size distributions corresponding to the runs at 120 or 300 rpm were rather similar and characterized by a very broad distribution ranging between 0.5 μm and several hundreds of microns, while the product recovered at the end of the synthesis applying a stirring rate of 600 rpm had a narrow size distribution, most of the particles, on a volume basis, having a size between 1 and 10 μm. The mean Kolmogorov microscale is also reported in Fig. 6. Whatever the shear rate applied, the majority of agglomerates were smaller than the corresponding micro-scale. This observation is in agreement with previous results from the literature showing that the size of flocs or aggregates resulting from a breakage process
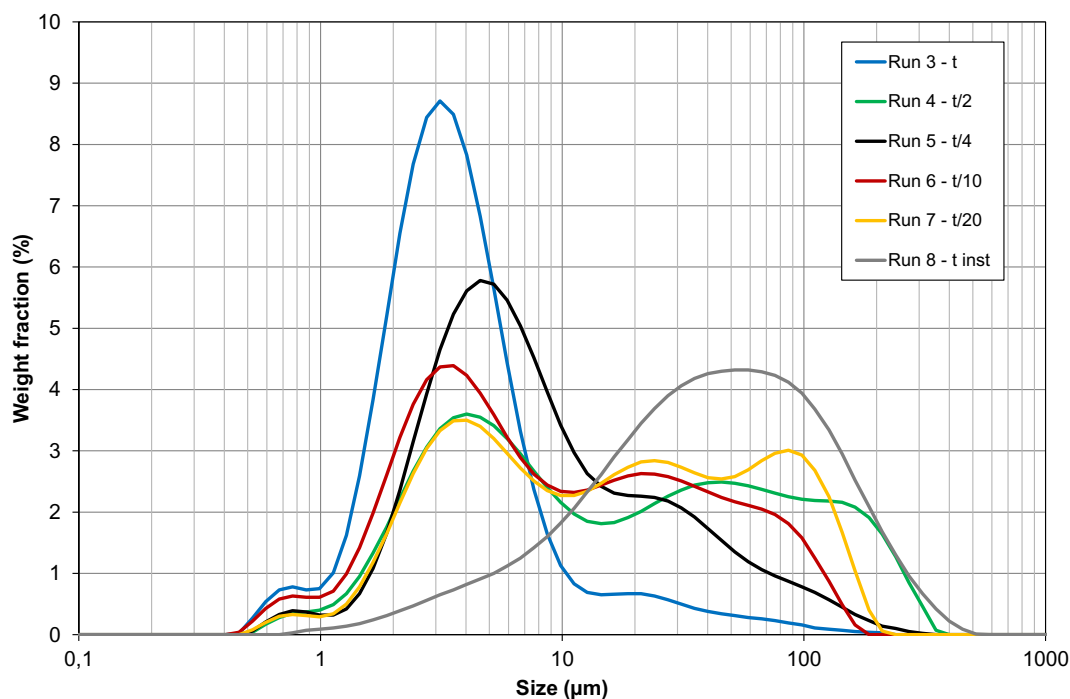
Fig. 8. Effect of the reactant flow rates or the synthesis duration on the particle size distribution.

is calibrated by the shear rate [15]. It can thus be concluded that the particle size distribution of HAP recovered at the end of the process is strongly dependent on the hydrodynamic conditions applied during the synthesis. Moreover, X-ray analysis of the calcined powder obtained during these runs revealed that the quality of the powder was improved when the stirring rate was increased. The corresponding Ca/P ratios, reported in Table 2, belong to the required standard range.

3.3. Effect of the reactant flow rate

The flow rate of reagents was also considered since it has an effect on the duration of the synthesis and thus on the productivity. The synthesis duration, initially fixed at 5 h for the reference synthesis described in the previous section, was reduced. Synthesis time was divided by 2, 4, 10 or 20 by increasing the reagent flow rates without changing their quantities. The time devoted to the feeding of the ammonia alone and the maturation time were also adapted to reduce the whole duration of the HAP synthesis. The synthesis duration labelled "t/inst" corresponds to a run in which all the reactants were introduced into the reactor quasi instantaneously. The experimental conditions for the different runs are summarized in Table 2. All these runs were performed at 75 °C with an agitation speed of the stirrer inside the reactor fixed to 600 rpm.

The reagent flow rates and the duration of the different steps of the synthesis procedure have an effect on the change of the pH over time, as is illustrated in Fig. 7. In Fig. 7a, the pH change is reported versus time from the beginning of the feeding of the three solutions: N, P and C, until the end of the synthesis. Whatever the process duration, the pH first increases due to the sole ammonia feed (not shown on the graphs) and then decreases, sharply during the first period and more slowly thereafter. Since the whole duration of synthesis changes depending on the run, Fig. 7b reports the change of pH over a dimensionless value of the process time, defined as the ratio of the actual process time minus the sole ammonia feeding duration to the whole synthesis duration. Fig. 7b reveals a difference in the drop of the pH, which finally lies between 7.5 and 8 depending on the process conditions.

Surprisingly, despite the change in the physicochemical conditions, the X-ray diffractograms of the calcined HAP powder were quite similar whatever the synthesis duration. As indicated in Table 2, the powder purity corresponded to the standard required level. However, an important effect of the synthesis duration was observed on the particle size distribution of the product recovered at the end of the synthesis (see Fig. 8). Whatever the process conditions, the size distributions were multimodal. The product contained a major population of particles having sizes of a few microns but the proportion of the coarser agglomerates increased as the synthesis duration decreased. A significant proportion of agglomerates were larger than the mean Kolmogorov microscale (equal to 45 µm at 600 rpm). It seems that the time needed to break the agglomerates was non-negligible. If all the reagents were put into the reactor quasi immediately (run t/inst), the product was even only composed of coarse agglomerates although the agitation speed of the stirrer was set to a high value, 600 rpm, to ensure good mixing of the reagents inside the reactor.

3.4. Effect of the stirring speed applied during the maturation step

Another important issue is to understand the impact of the maturation step usually performed in industrial practice. To demonstrate the change of the particle size during this step, a run was performed at 300 rpm and the reagents were added over a period of 30 min (experimental conditions referenced as synthesis t/10). The maturation step was then performed by setting the stirrer speed at 600 rpm to highlight the effect of the stirring conditions during this step, and samples were withdrawn after different periods of time from 0 (no maturation at all) to 90 min. The evolution of the product size distributions is plotted as a function of the maturation time (t_mat) in Fig. 9a. It is clear that the size distribution was still evolving during the maturation step. The largest agglomerates were broken, giving birth to smaller ones, and the proportions of particles having sizes around a few microns and around 0.8 µm progressively increased. It is also interesting to note that the modes of the sub-populations did not change to any great extent, suggesting that the size reduction mechanism was most probably a de-agglomeration rather than a true breakage process. However, globally speaking, the change of the product size distribution during the maturation step, even performed at a high stirring speed, was not very significant. After 1 h and a half, the proportion of coarse agglomerates was still very high. In addition, a comparison of the product size distributions of samples synthesized with a stirrer speed of 300 rpm before the maturation step or after a maturation step performed at 300 (Run 9) or 600 rpm (Run 10) are compared in Fig. 9b. The product size distribution for a run performed at 600 rpm without maturation (Run 6) is also reported. It can be seen that the maturation step had a small effect on the product size distribution. However, this effect was greater when the stirrer speed during maturation was higher but all these effects were small compared to the impact of the stirring conditions during the synthesis. So, it can be concluded that the stirring conditions during the precipitation step are of prime importance. When the reagent feeding is finished, the product size distribution hardly evolves, agglomerates being hard enough to resist shearing conditions.

3.5. Effect of the physicochemical parameters

The physicochemical conditions, notably the temperature and pH, are known to be key parameters for obtaining the desired apatite compound [6,10,11,14]. Since the pH changes during reagent feeding depend on the flow rates, special attention was paid to this parameter. In the standard HAP synthesis described in Section 2.1, ammonia was initially fed to increase the pH of the reaction medium prior to the addition of the two principal reagents, phosphoric acid and calcium nitrate. A series of runs was performed with increasing amounts of ammonia. By changing the flow rate, the amount of ammonia was set to 1.4 times (Run 12) and 3 times higher (Run 13) than the rate used previously (Run 11), the other parameters being kept constant (synthesis duration t/2 and stirring speed 300 rpm). The evolution of the pH versus the process time is reported in Fig. 10a. The dotted vertical lines delimit the period during which the N, P and C solutions were fed. During the period in which only ammonia was fed (on the left of the first vertical line), the higher the ammonia amount was, the higher was the increase of the pH. However, the gap was above all significant for the run performed with the highest quantity
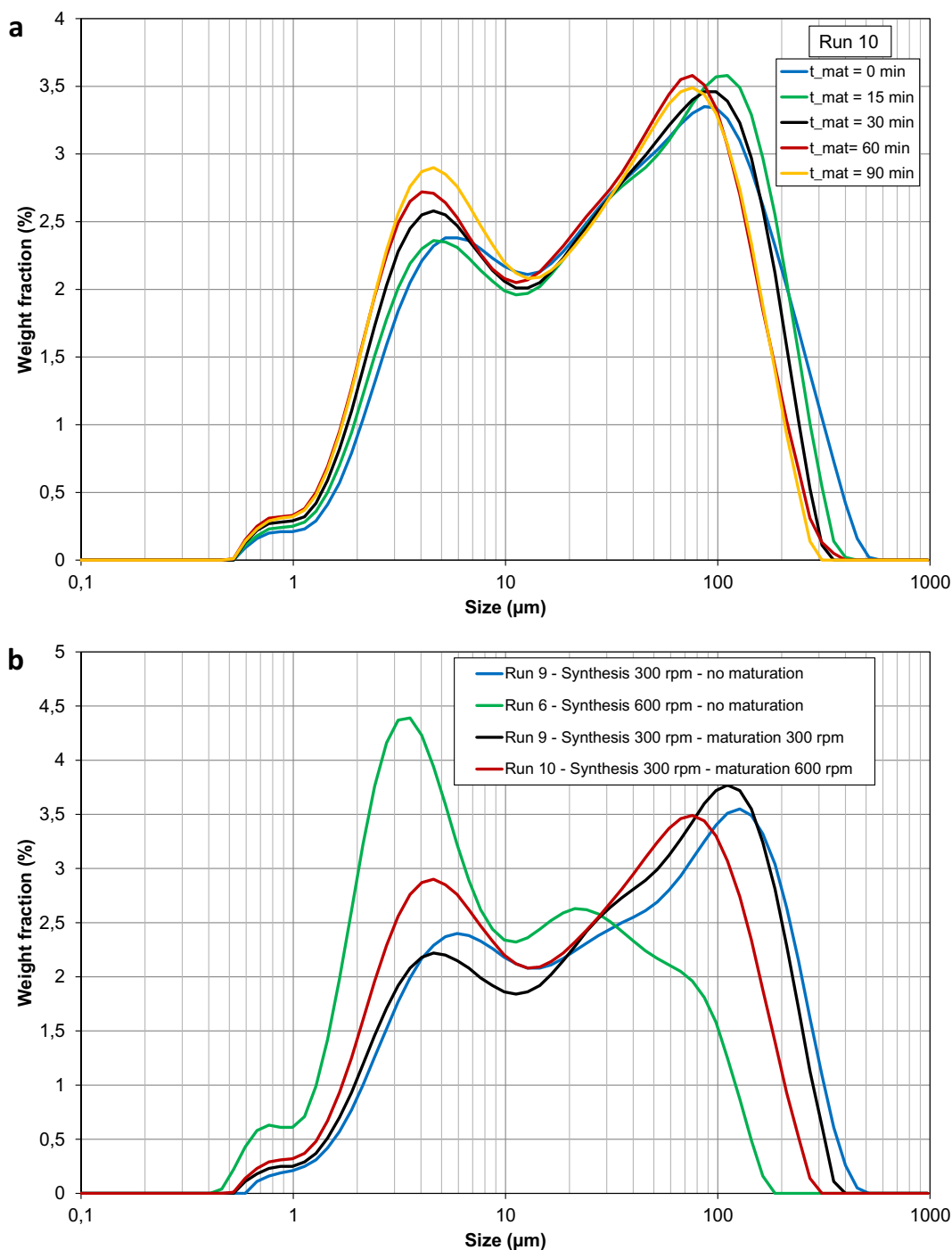
Fig. 9. Effect of stirrer speed during maturation step. a) Effect of maturation duration on particle size distribution (Run 10). b) Comparison of impact of stirring rate during synthesis and maturation steps.

of ammonia, compared to the other two conditions. The HAP properties are shown in Fig. 10b. Whereas no significant change of the purity was noticed (cf. Table 2), an important effect on the product size distribution was again brought to light. The greater the amount of ammonia was, i.e. the more basic the pH, the coarser were the agglomerates obtained at the end of the synthesis and the greater was the spread of the size distribution.

4. Towards an optimization of the HAP synthesis

4.1. pH regulation around a constant value

Since the addition of ammonia showed an important effect on the aggregate size distribution, other runs were conducted with the pH maintained at a constant value (Run 14   pH = 8 or Run 15   pH = 9) thanks to pH regulation, as has been done in various previous studies [9,11,12,14]. The size distributions of the product recovered at the end of the syntheses are reported in Fig. 11. As expected, the product size distribution depended strongly on the pH, in a sim ilar way to what was reported previously when the amount of am monia was changed. The HAP purity, as revealed by the Ca/P ratios in Table 2, was also within the desired standard range. pH, rather than ammonia amount, is the key physicochemical parameter that has an effect on HAP properties. Decreasing pH may thus allow the agglomerate size to be decreased and reduce the spread of the distribution.
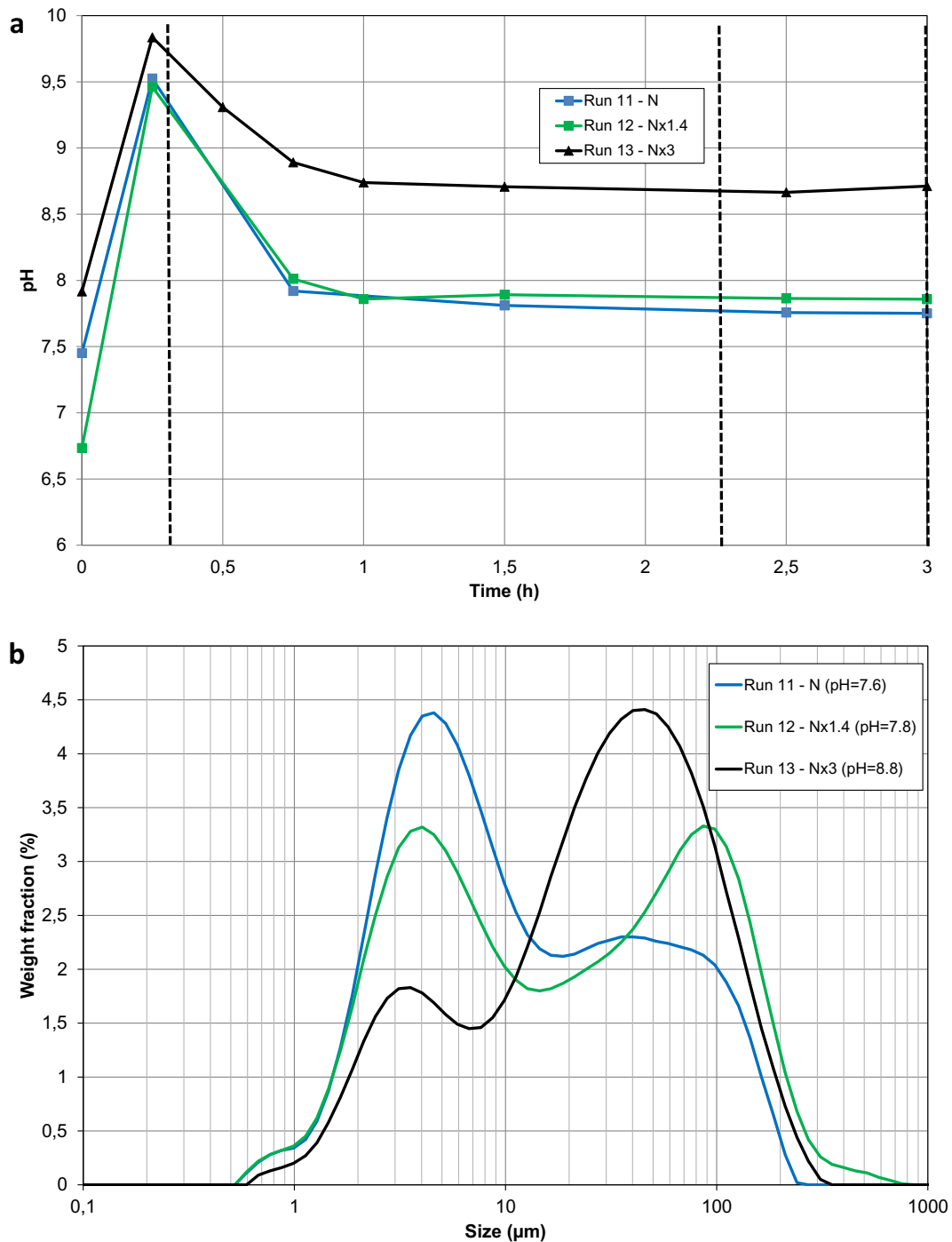
Fig. 10. Effect of ammonia addition on HAP properties. a) Change of pH over time depending on the ammonia content in the reactant feed. b) Effect of ammonia content on size distribution of the product recovered at the end of synthesis.

4.2. pH regulation with an imposed profile

In order to reduce the process duration while obtaining a narrow size distribution, a decrease of the pH appeared pertinent. However, as previously mentioned in the literature, a minimum pH value of about 7 is needed to obtain pure HAP. So, a pH regulation (Titrino 848 + from Metrohm) was performed following a specific profile in which the pH was decreased for only a short period during the first few minutes of the synthesis process, as large agglomerates are formed quasi instantaneously. For this run (Run 16), the stirring speed was

kept constant at 600 rpm, the temperature was 75 °C and the reagent flow rates were imposed as indicated in Table 2 in order to obtain a du ration of 30 min for the whole synthesis (t/10). The pH was initially set to 7.5 but, after 1 min of the process, the ammonia feed was stopped while the other reactant flow rates were maintained constant. In this way, large agglomerates were broken into smaller pieces since an acidic medium led to increased HAP solubility, promoting the breakage of fragile bonds inside the agglomerates. Then the ammonia feed was turned on again and a pH level of 7.5 was imposed until the end of the synthesis in order to avoid the formation of a non stoichiometric
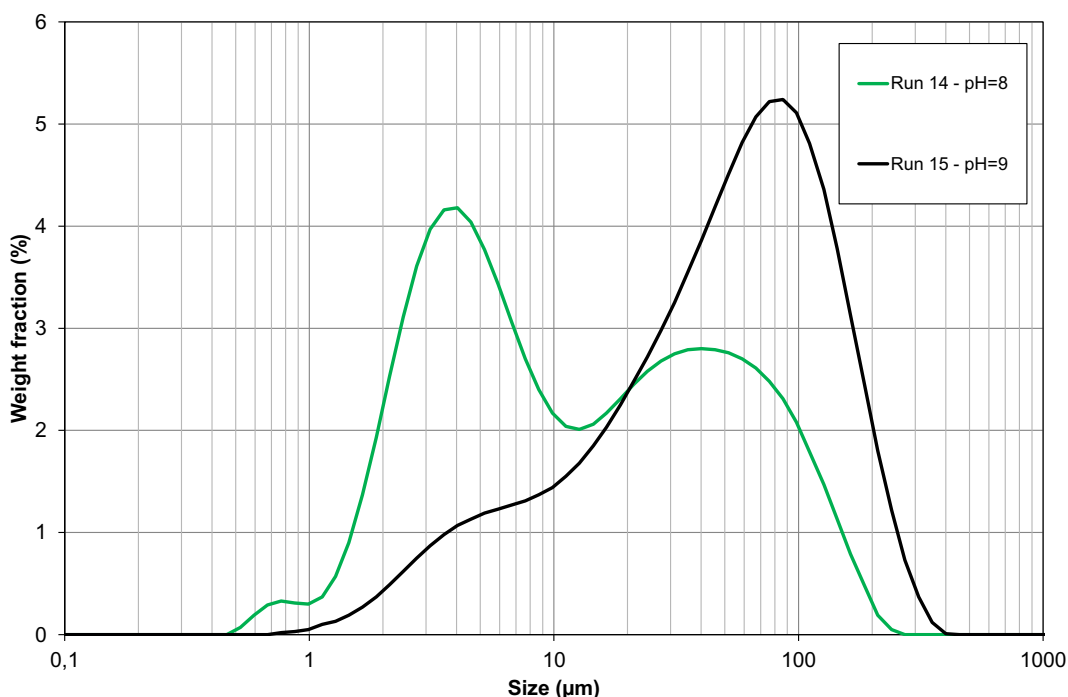
Fig. 11. Effect of pH on agglomerate size distribution of the product recovered at the end of the synthesis.

calcium phosphate. The resulting pH profile is given in Fig. 12a. The particle size distribution of the product recovered at the end of the synthesis is reported in Fig. 12b and compared with the properties of the product obtained when performing syntheses without pH regulation, with two different durations: t or t/10. The other conditions were kept the same (600 rpm, 75 °C).

It is clear that the agglomerates produced by imposing a pH profile were smaller than those obtained in the same experimental conditions but without pH regulation. With pH regulation, the vast majority of agglomerates were between 1 and 20 μm with a mode around 5.5 μm. A small sub population of fines around 0.8 μm still existed, as did another sub population of large particles having sizes between 20 and 100 μm, probably made up of agglomerates that were not broken. Nevertheless, the agglomerate size distribution was narrow and satisfied the HAP requirement. Moreover, as can be checked on the values reported in Table 2, the HAP quality, even with a Ca/P ratio slightly lower than the target for perfectly stoichiometric HAP (1.667), lay in the desired standard range for syntheses carried out with or without pH regulation. Fig. 13 reports typical SEM photos of the agglomerated powder recovered after synthesis without pH regulation and for a standard duration (Run 3) (cf. Fig. 13a) or for the run performed with pH regulation and a duration ten times shorter (Run 16) (cf. Fig. 13b). Quite similar structures could be observed whatever the magnification although, when pH regulation was applied, agglomerates seemed to be more compact and composed of many acicular crystallites, like a sea urchin, whereas, without pH regulation, the assemblies appeared to be more disordered. In any case, both structures are suitable for the biomaterial application.

5. Conclusions

Stoichiometric HAP synthesis was studied by varying physico chemical and hydrodynamic conditions and analysing their effect on both the size distribution of the agglomerate and the chemical composition of the product. A reference synthesis was defined, based on a scale down of the usual industrial practice for HAP production. The reference synthesis was used as a basis for suggesting improvements, keeping in mind throughout this study that stoichiometric HAP, with a purity of at least 95%, and a narrow agglomerate size distribution, was required. The following main conclusions can be drawn:

A rather high stirring rate is needed to mix the reactants properly and obtain a product with a narrow size distribution around a few microns. Most of the agglomerates are smaller than the mean Kolmogorov microscale calculated on the basis of the mean shear rate imposed during the precipitation.

The whole duration of the synthesis can be strongly reduced without affecting the chemical purity of the product but the pH must be properly regulated, by allowing it to become acidic for a very short period of time just after the formation of large agglomerates and then setting it at over 7.5 again to avoid the formation of non stoichiometric calcium phosphate.

The maturation step has only a slight effect on the size distribution and could be avoided for high enough synthesis temperatures, as suggested by previous literature.

Notation

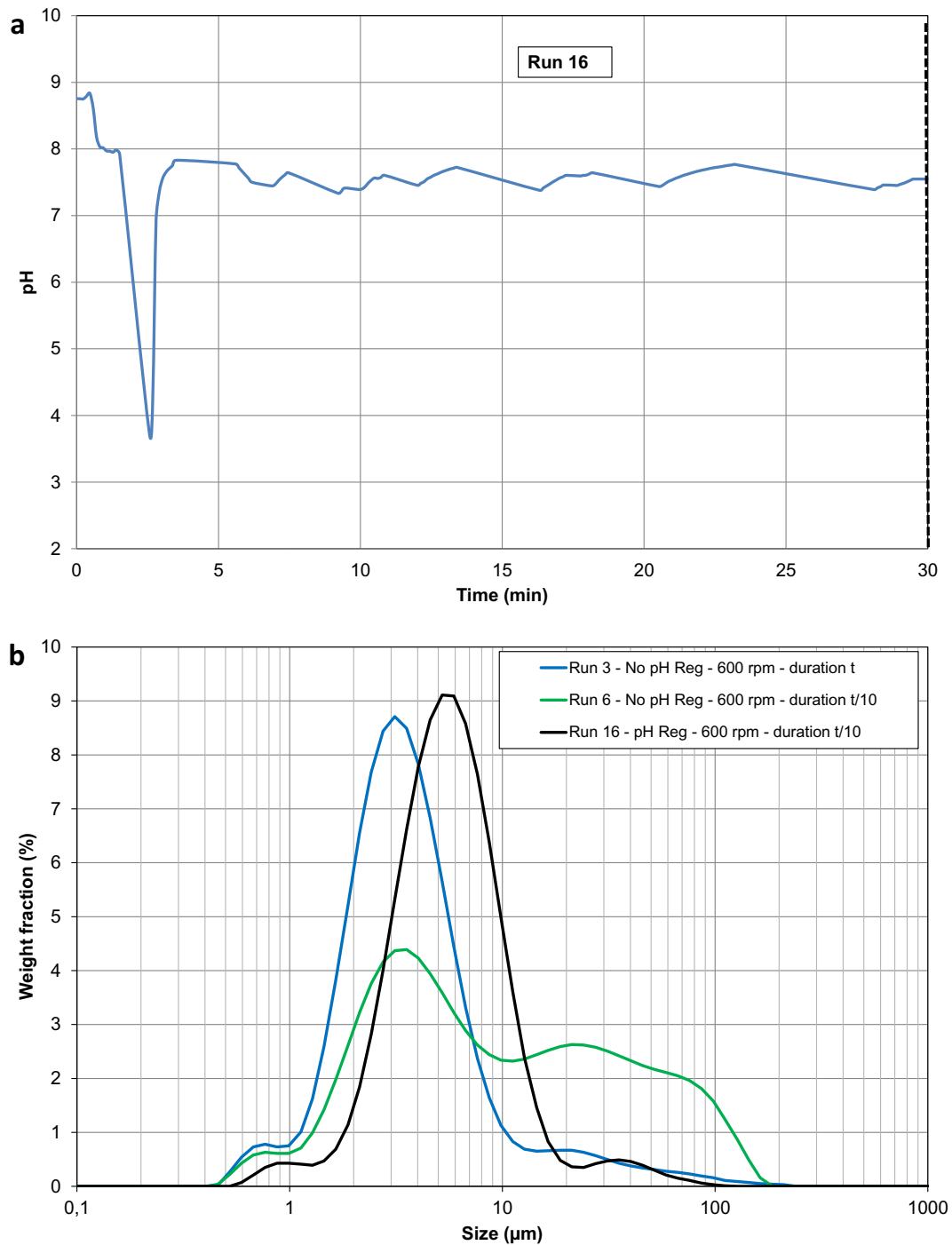|	
CaO	calcium oxide
Ca/P	calcium phosphate ratio
HAP	stoichiometric hydroxyapatite
α TCP	alpha tricalcium phosphate
β TCP	beta tricalcium phosphate

Fig. 12. pH profile regulation and properties of the product recovered at the end of the syntheses with or without pH regulation.

List of symbols

d_a	impeller diameter, [m]
G	global velocity gradient, [s^{-1}]
M_x	molar weight of product x, [kg·mol^{-1}]
n_x	mole number of product x, [−]
N	impeller frequency, [rpm]
N_p	power number [−]
P	global power dissipated in the reactor, [W]
Re	Reynolds number, [−]
V	volume of the suspension, [m^3]
w_x	mass fraction of product x, [kg]
ν	kinematic viscosity, [m^2.s^{-1}]
ρ	density of the suspension, [kg.m^{-3}]
$\langle\varepsilon\rangle$	global viscous dissipation rate of the turbulent kinetic energy, [m^2.s^{-3}]
$\langle\eta\rangle$	mean Kolmogorov microscale, [m]
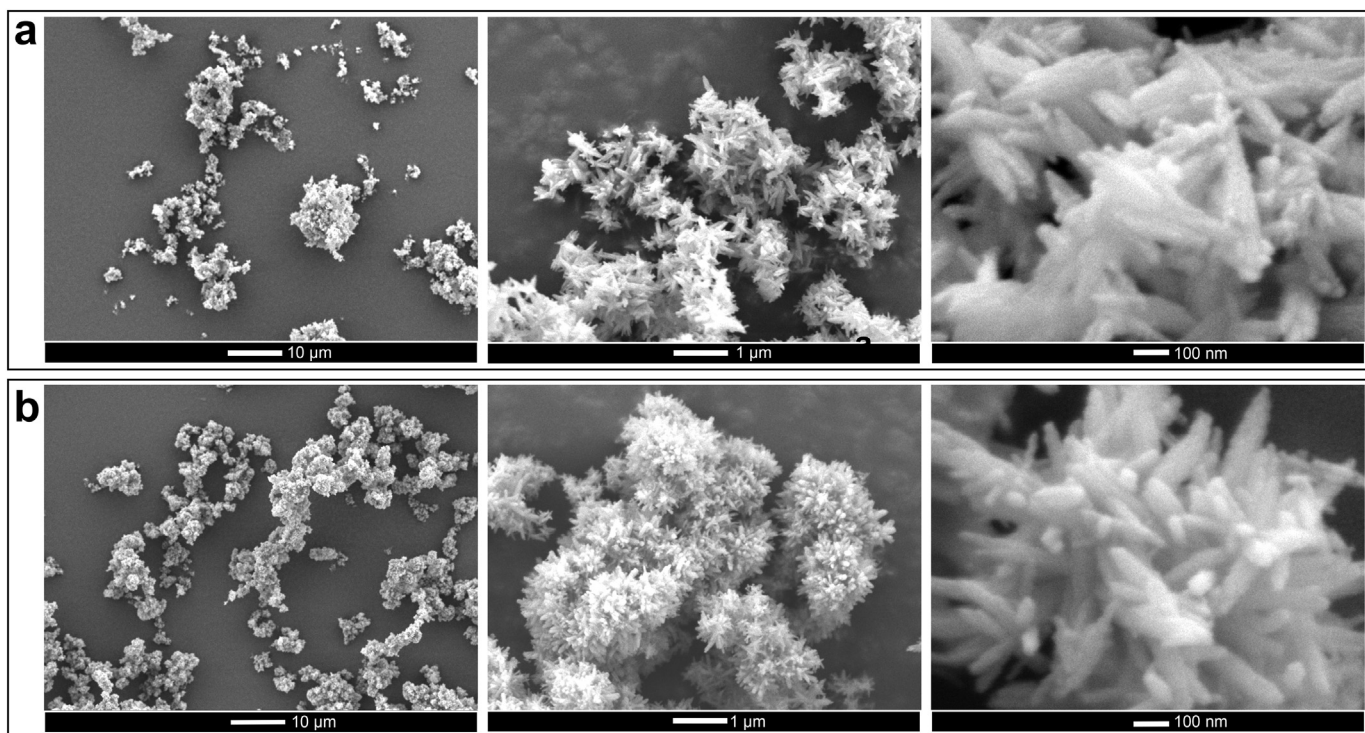
Fig. 13. SEM photos of the agglomerated powder recovered after synthesis. a) without pH regulation (Run 3). b) with pH regulation (Run 16).

References

[1] J.C. Elliott, Structure and Chemistry of the Apatites and Other Calcium Orthophosphates, Elsevier Amsterdam, 1994.

[2] C. Rey, Calcium phosphates for medical applications, Calcium Phosphates I Biological and Industrial Systems, Springer 1998, pp. 217–251.

[3] C. Rey, C. Combes, C. Drouet, D. Grossin, Bioactive ceramics: physical chemistry, in: P. Ducheyne (Ed.), Comprehensive Biomaterials, Elsevier, Oxford 2011, pp. 187–221.

[4] A.K. Nayak, Hydroxyapatite synthesis methodologies: an overview, Int. J. Chem. Res. 2/2 (2010) 903–907.

[5] N.Y. Mostafa, Characterization, thermal stability and sintering of hydroxyapatite powders prepared by different routes, Mater. Chem. Phys. 94 (2005) 333–341.

[6] S. Lazic, S. Zec, N. Miljevic, S. Milonjic, The effect of temperature on the properties of hydroxyapatite precipitated from calcium hydroxide and phosphoric acid, Thermochim. Acta 374 (2002) 13–22.

[7] M.R. Saeri, A. Afshar, M. Ghorbani, N. Ehsani, C.C. Sorrell, The wet precipitation process of hydroxyapatite, Mater. Lett. 57 (2003) 4064–4069.

[8] P. Lou, T.G. Nieh, Preparing hydroxyapatite powders with controlled morphology, Biomaterials 17 (1996) 1959–1964.

[9] R. Rodriguez-Clemente, A. Lopez-Macipe, J. Gomez-Morales, J. Torrent-Burgues, V.M. Castano, Hydroxyapatite precipitation: a case of nucleation-aggregation-agglomeration-growth mechanism, J. Eur. Ceram. Soc. 18 (1998) 1351–1356.

[10] C. Liu, Y. Huang, W. Shen, J. Cui, Kinetics of hydroxyapatite precipitation at pH 10 to 11, Biomaterials 22 (2001) 301–306.

[11] N.S. Al-Qasas, S. Rohani, Synthesis of pure hydroxyapatite and the effect of synthesis conditions son its yield, crystallinity, morphology and mean particle size, Separ. Sci. Technol. 40 (2005) 3187–3224.

[12] J. Gomez-Morales, J. Torrent-Burgues, T. Boix, J. Fraile, R. Rodriguez-Clemente, Precipitation of stoichiometric hydroxyapatite by a continuous method, Cryst. Res. Technol. 36 (2001) 15–36.

[13] I. Mobasherpour, M. Soulati Heshajin, A. Kazemzadeh, M. Zakeri, Synthesis of nano-crystalline hydroxyapatite by using precipitation method, J. Alloy. Comp. 430 (2007) 330–333.

[14] A. Afshar, M. Ghorbani, N. Ehsani, M.R. Saeri, C.C. Sorrell, Some important factors in the wet precipitation process of hydroxyapatite, Mater. Des. 24 (2003) 197–202.

[15] C. Coufort, C. Dumas, D. Bouyer, A. Liné, Analysis of floc size distributions in a mixing tank, Chem. Eng. Process: Process Intens. 47 (3) (2008) 287–294.